CHAPTER 4

CHARACTERIZATION RESULTS

In this chapter, the analysis of structural, thermal, mechanical, and electrochemical properties has been discussed in detail for all prepared gel polymer electrolytes.

Different characterization techniques such as X-ray diffraction, differential scanning calorimetry, scanning electron microscopy, atomic force microscopy, and fourier transforms infrared spectroscopy have been used to analyze structural and thermal properties. Electrochemical properties and cyclic voltammetry are also carried out. The mechanical properties such as tensile strength of the gel polymer electrolytes have been investigated.

4.1 X-ray Diffraction Analysis

XRD technique is supreme to analyse the detailed information regarding the structure of the materials including the coordination between the ion and polymers in the polymer electrolytes [1]. The nature of the polymer can be estimated by analyzing the amorphous peak or crystalline peaks from the XRD spectra and whether the complex formation is taking place between the present constituents in the gel polymer electrolyte such as a polymer, salt, plasticizers, nanofiller, etc., can also be studied. XRD patterns of the polymer contain both sharp peaks corresponding to crystalline regions and broad halos correspond to amorphous phases. The structure of the polymer electrolyte system is expected to have amorphous nature as ion transport takes place in the polymer electrolyte through the amorphous phase of polymer-salt complexes.

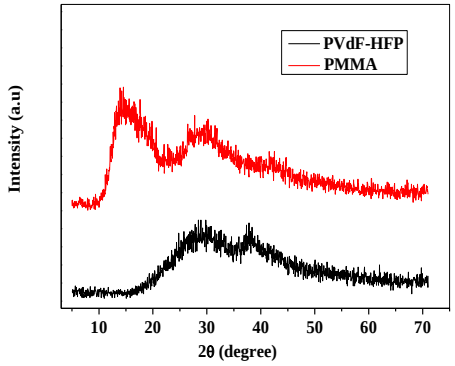

Figure 4.1 XRD pattern of pure PVDF-HFP and PMMA

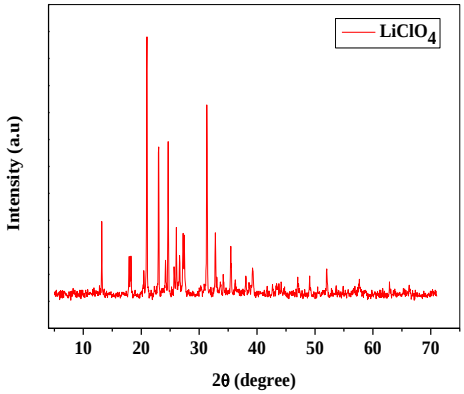

Figure 4.2 XRD pattern of $LiClO_4$

The XRD patterns of Pure PVDF-HFP and PMMA are recorded and shown in Figure 4.1. Two peaks at 29.7° and 38.3° for the pure PVDF-HFP film have been observed, which confirmed the partial crystallization of PVDF units in the copolymer and overall its semi-crystalline nature [2]. The pattern for pure PMMA shows a broad and less intensive peak at 2θ ≈13.8° and ≈ 29° which indicates the complete amorphous nature of the PMMA film [3]. The XRD pattern of pure $LiClO_4$ salt is depicted in Figure 4.2. The Diffraction pattern of $LiClO_4$ shows high intense characteristic peaks which revealed the crystalline nature of the salt [4].

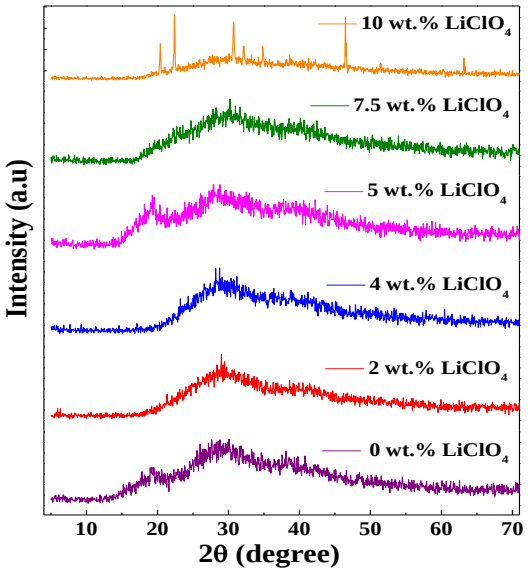

Figure 4.3 XRD pattern of GPE system with different concentrations of $LiClO_4$ - Series (a).

Figure 4.3 shows the XRD diffraction pattern of PVDF-HFP:PMMA- PC:DEC - $LiClO_4$ films (Series a) with different concentrations of $LiClO_4$. From the XRD pattern of GPE

samples, it is revealed that the absence of crystalline peaks pertaining to $LiClO_4$ in the polymer complexes confirms the complex formation which seems to occur only in the amorphous phase [5] which confirms the complete dissolution of the salts in the complex matrix, implying that the salt does not have any separate phases in the electrolyte. The prominent peak of PMMA at 13.8° disappeared and the intense peaks $2\theta \approx 29.7°, 38.3°$ of PVDF-HFP decreased together with the broadening up to the incorporation of 7.5 wt.% $LiClO_4$ which indicates the increase in the amorphicity of the films. Mahendran et al. reported less crystallinity in PMMA - PVdF – $LiClO_4$ – DMP system and compared with systems containing $LiCF_3SO_3$ and $LiBF_4$ salt. It is reported that the less crystalline nature of the film may be due to loose packing between macromolecular chains of the polymer matrix [6]. In the present gel polymer electrolyte system, the amorphous phase is maintained up to 7.5wt.% $LiClO_4$ and on further addition, the sharp peaks of $LiClO_4$ salt have appeared which indicates the crystallinity of the complex increases. This may be due to the aggregation of Li^+ and ClO_4^- ions as a result of increased free charge carriers. A similar feature has also been observed by Pradeepa et al. [7].

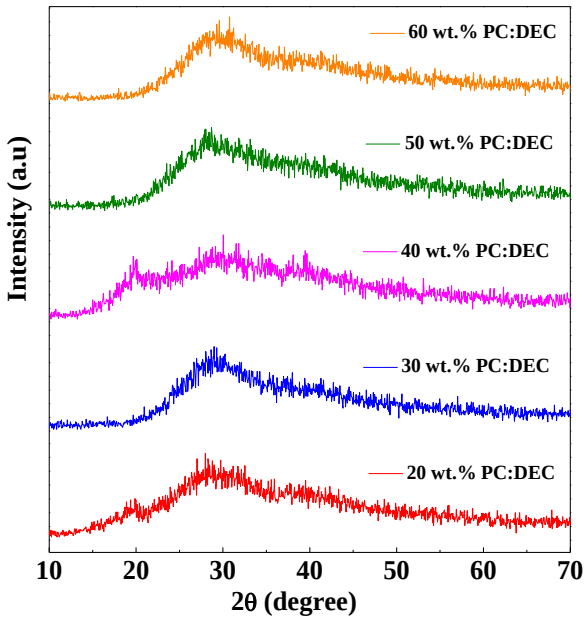

Figure 4.4 XRD pattern of GPE system with different concentrations of PC:DEC – Series (b)

The effect of plasticizers in the gel polymer electrolyte, the XRD study is carried out with the varying amount of propylene carbonate (PC) and diethyl carbonate (DEC) from 20 wt.% to 60 wt.% in the PVDF-HFP:PMMA - $LiClO_4$ electrolyte system. XRD pattern of GPE membranes (Series b) with different concentrations of PC:DEC plasticizers are

shown in Figure 4.4. XRD patterns do not show any characteristic peak of $LiClO_4$ salt indicating the complete dissolution of lithium salt in the polymer matrix [8]. XRD diffraction patterns show no X-ray peaks except a broad hump at about 29°. The increase in the height of hump along with broadening is observed as the amount of PC:DEC plasticizers is added from 20 to 60 wt.%, which attributes to the increasing amorphous nature of the GPE films. Low molecular weight plasticizers PC:DEC promotes the separation of inter and intra-chains due to trapping of plasticizers into polymer matrix [8]. Song et al. reported a similar trend in 85PVDF–HFP:15$LiBF_4$ + x wt.% (EC + PC) systems in which EC:PC has been taken but the amount of plasticizer was kept at 200 wt.% [9]. According to Song et al., a small-molecule of plasticizer, when added into the polymer, interrupts the crystalline nature of the polymer which decreases the crystallinity of GPE films shown in the X-ray pattern.

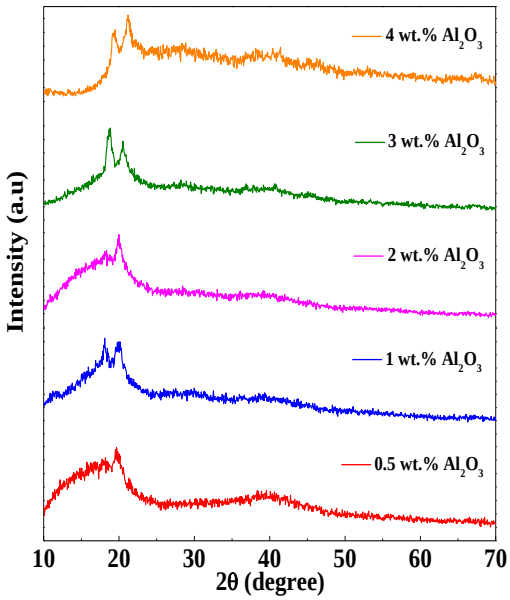

Figure 4.5 XRD analysis of GPE with various amount of Al_2O_3 nano-filler - Series (c).

The electrochemical and mechanical properties of the gel polymer electrolyte can be enhanced by dispersing the nano-particles. Because of the large surface area of nanoparticles also called fillers, prevent the reorganization of the local chain which results in a high degree of disorder structure and an amorphous phase is achieved in the matrix. A varying amount of Al_2O_3 nano-filler in an optimized sample of the second series for which a high conductivity value is found has been undertaken.

Figure 4.5 shows the X-ray pattern of the gel polymer electrolyte films with different amounts of nano-filler Al_2O_3. To get insight into the structural variation of the nanocomposite gel polymer electrolyte (NCGPE), it is worth first look at the XRD pattern of pristine materials. The characteristic peaks of $LiClO_4$ and Al_2O_3 nano-particles are not exhibited by the XRD pattern of the NCGPE [10]. The broad nature of peaks shows the overall amorphous nature. The trapped nano-particles having a large surface area that prevent the polymer chain from reorienting, in turn, enhances the degree of disorder. This may be due to the present Lewis acid surface group of Al_2O_3 nano-filler interact with the polymer and salt which reduces the ion coupling between them [11]. The increase in the amorphicity with an increase in the Al_2O_3 nanofiller up to 2 wt.% in the GPE system is observed. This also suggests that the ion-dipolar complex can accommodate Al_2O_3 nanoparticles up to 2 wt.%. The reduction in the crystalline nature of PVDF-HFP:PMMA based gel polymer electrolytes system up to 6 wt.% Al_2O_3 nanofiller has also been reported by Mishra et al.[12]. In our study, beyond the 2 wt.% Al_2O_3 nano-filler, two peaks with high intensity at $2\theta \approx 18°$ and 21° have appeared which is an indication of a decrease in amorphous phase due to aggregation of Al_2O_3 nanofiller.

4.2 SEM Analysis

The scanning electron microscope (SEM) examines the microstructure morphology of the sample. The morphology of the polymer electrolyte is a useful parameter to probe the presence of the amorphous region, structure on the surface of the filler after blending, mixing the salt or dispersion of the nanofillers, etc. In the present work, the study of the morphology of the gel polymer electrolyte samples of all three series is undertaken.

Surface morphology of the GPE films with $LiClO_4$ salt containing 2 wt.% to 10 wt.% is shown in Figure 4.6. The image shows uniformly distributed spherical structures in the GPE film with 2 wt.% $LiClO_4$. It shows a normal porous surface with small pore size. The morphology changes to greater pore size when 7.5 wt.% of $LiClO_4$ is doped into the polymer electrolyte. The pores in the polymer complexes help in trapping a large amount of electrolyte solution. Due to this, the swelled nature of the GPE has been observed containing 7.5 wt.% of $LiClO_4$. The observed feature is very similar to those reported by Ramesh et al.[13]. These microstructures lead to better-conducting pathways for Li^+ ions and consequently lead to higher ionic conductivity.

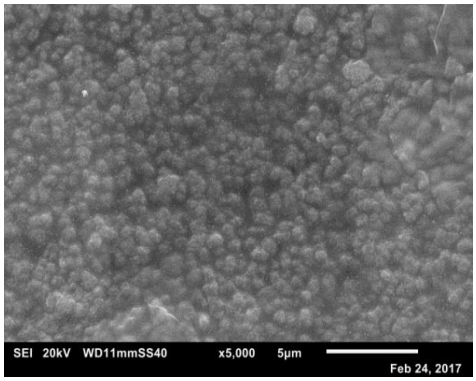

(a) 2 wt% $LiClO_4$

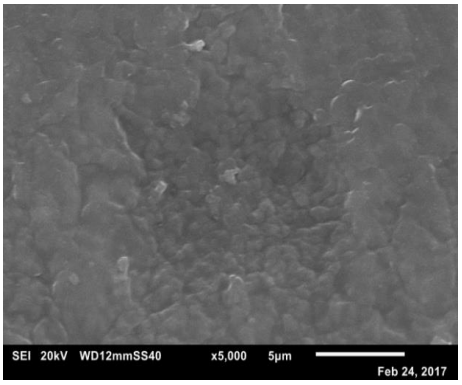

(b) 4 wt% $LiClO_4$

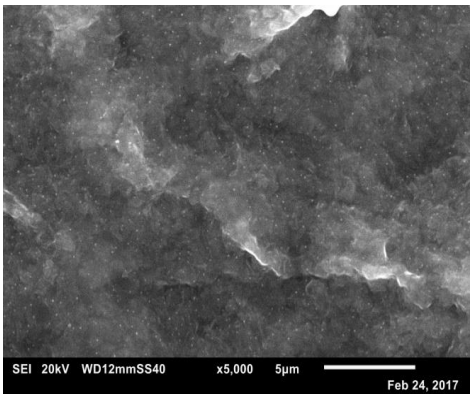

(c) 5 wt% $LiClO_4$

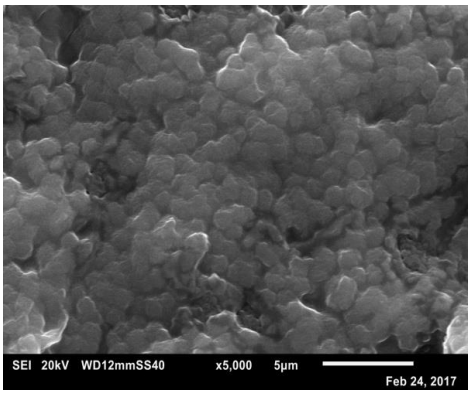

(d) 7.5 wt% $LiClO_4$

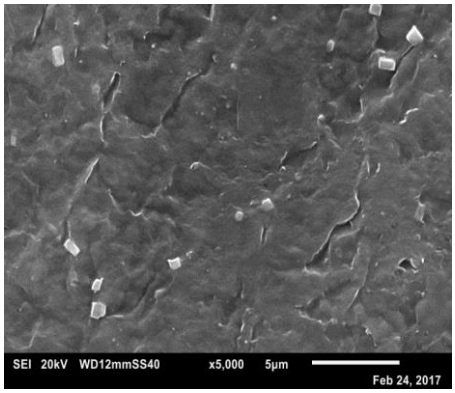

(e) 10 wt% $LiClO_4$

Figure 4.6 SEM micrographs of GPE system with different concentrations of $LiClO_4$ - Series (a).

Similarly, to investigate the change in the morphology due to the addition of PC:DEC plasticizers, the SEM micrographs are shown in Figure 4.7. Microspores with large size have been observed in the GPE with a lower amount of plasticizers i.e. 20 wt% PC: DEC. It reveals that these micropores are not filled with the liquid electrolyte due to an insufficient amount of PC:DEC. Addition of more amount of PC:DEC plasticizers to polymer electrolyte enhances more number of embedded small pores with swelled nature of GPE. These micropores filled with liquid electrolytes provide the conducting pathway for transportation of lithium-ions [14]. This observation has been reported by Senthil

Kumar et al. [15] in their study on plasticized PVDF−HFP/PEMA blended polymer electrolyte. However, in our case, surface morphology shows the remarkably increase in swelled nature of the film by incorporating a higher amount of plasticizer.

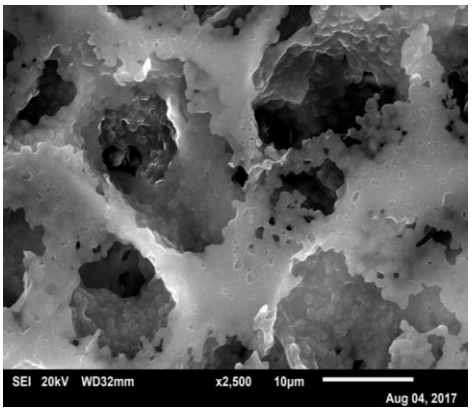

(a) 20 wt% PC:DEC

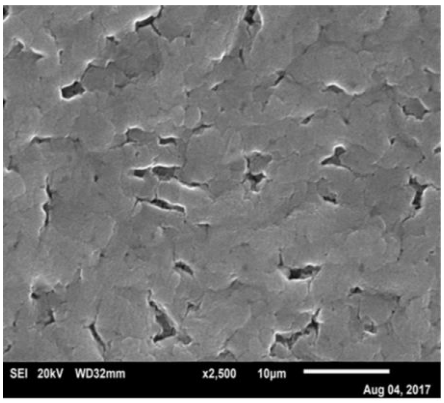

(b) 30 wt% PC:DEC

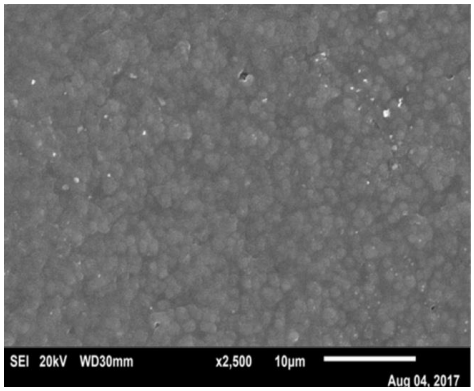

(c) 40 wt% PC:DEC

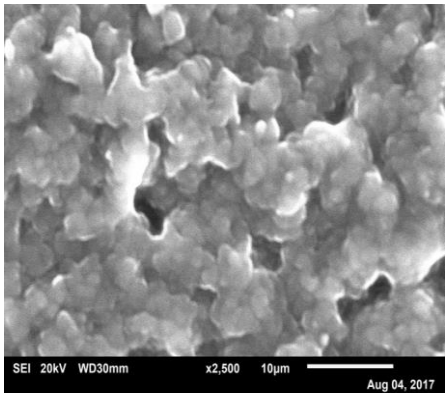

(d) 50 wt% PC:DEC

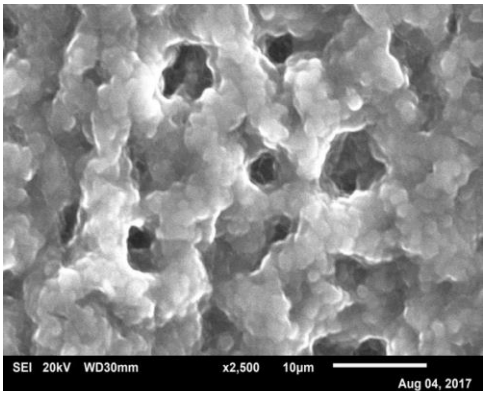

(e) 60 wt% PC:DEC

Figure 4.7 SEM micrographs of GPE system with different concentrations of PC:DEC - Series (b).

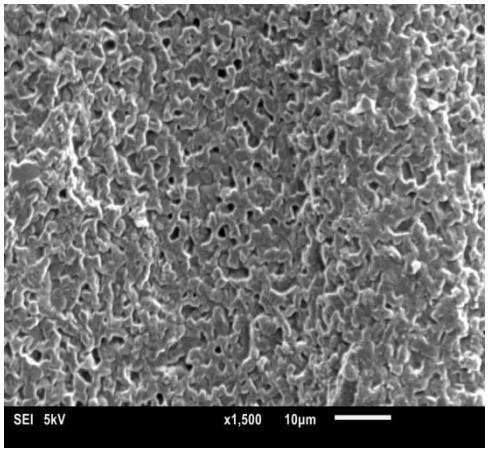

(a) 0.5 wt% Al_2O_3

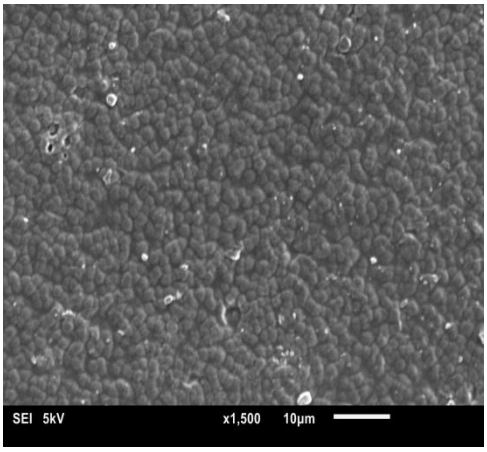

(b) 1 wt% Al_2O_3

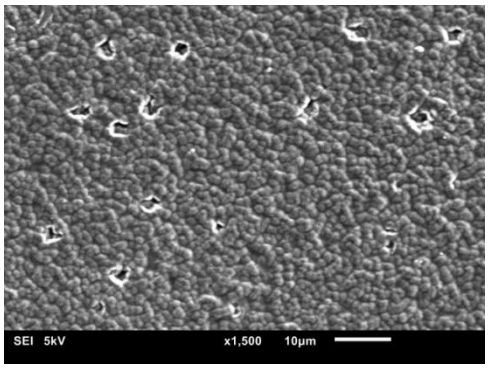

(c) 2 wt% Al_2O_3

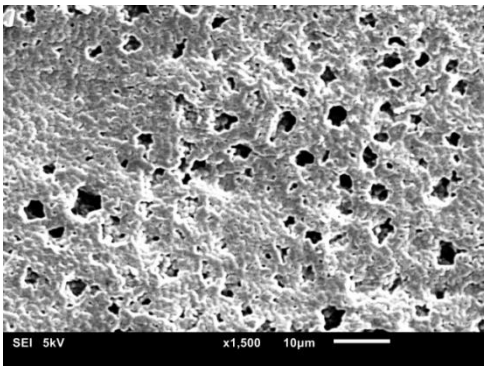

(d) 3 wt% Al_2O_3

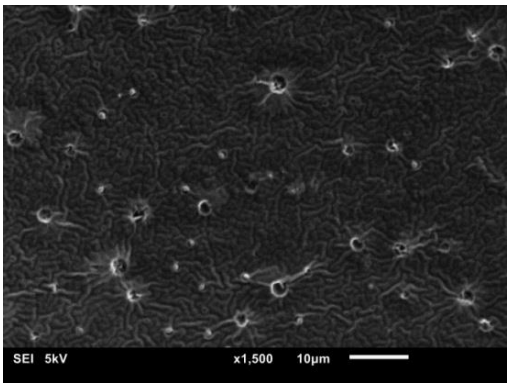

(e) 4 wt% Al_2O_3

Figure 4.8 SEM micrographs of nanocomposite GPE system with different concentrations of Al_2O_3 - Series (c).

Now, the morphology of the present GPE system in which nanofillers Al_2O_3 have been dispersed and has been carried out by SEM. Figure 4.8 depicts the SEM micrograph of the films with different concentrations of nano-filler Al_2O_3. The surface morphology substantially changes with the addition of nanoparticles. A very different nature of morphology has been observed for the GPE film having a lower amount of nano-filler i.e. 0.5 wt.% Al_2O_3. With an increasing amount of the nanofiller, the pore size gets smaller, but the number of pores is uniformly increased which has a better ability of retention of

liquid electrolyte. These uniformly connecting pores provide the conduction path for the mobility of ions. Rao et al. in PI/PVDF-HFP/Al_2O_3 GPE system have discussed the improvement of electrolyte uptake ability and cyclic stability [16]. At 2 wt.% Al_2O_3 nano-filler, the pores are filled by nanofillers in the polymer matrix. This helps for the dissociation of anion-cation pairs of $LiClO_4$ salt and increases the charge carriers. Mishra et al. reported that without nano-filler, the films contain pores and are filled after dispersed nanoparticles into a polymer matrix resulting in dissociation of the cation-anion pair for conduction of free charge carriers [12]. Above 2 wt.% Al_2O_3 concentration, the disappearance of uniformly distributed pores may be due to aggregation of nano-particles or aggregation of dissociated ions.

4.3 DSC Analysis

As thermal properties such as glass transition temperature, melting point, and thermal stability are the important parameters resulting from the morphology and microstructure of the electrolyte sample. These parameters affect the working of the battery when a sample is used as a separator. The mechanical properties such as softening or melting of the electrolytes often change with change in operational temperatures of the battery causing a short circuit between anode and cathode which ultimately results in the explosion of the battery. Under this situation, it is necessary to investigate the thermal properties of the sample [17].

In the present study, thermal properties have been investigated using the differential scanning calorimetry (DSC) technique. The thermal properties of pure PVDF-HFP film, pure PMMA film, PVDF-HFP:PMMA film, and all gel polymer electrolyte systems with different concentrations of $LiClO_4$, PC:DEC, and Al_2O_3 have been carried out. Figure 4.9 (a to c) shows the DSC thermograph of pure PVDF-HFP, pure PMMA, and PVDF-HFP: PMMA respectively. The endothermic peak at 137.09 °C is exhibited by pure PVDF-HFP which is ascribed to its melting temperature [18]. For the pure PMMA, the melting temperature is recorded at 142.80 °C. It is believed that the conduction of ions takes place easily through the amorphous region of the system. For the blend film of PVDF-HFP:PMMA, the endothermic peak corresponds to the melting point of the blend is recorded at 132.59 °C which is different from both the polymer constituents. Compared to

pure polymers, the melting temperature of the blend is found at a lower temperature which indicates the mixing of the blending of polymers.

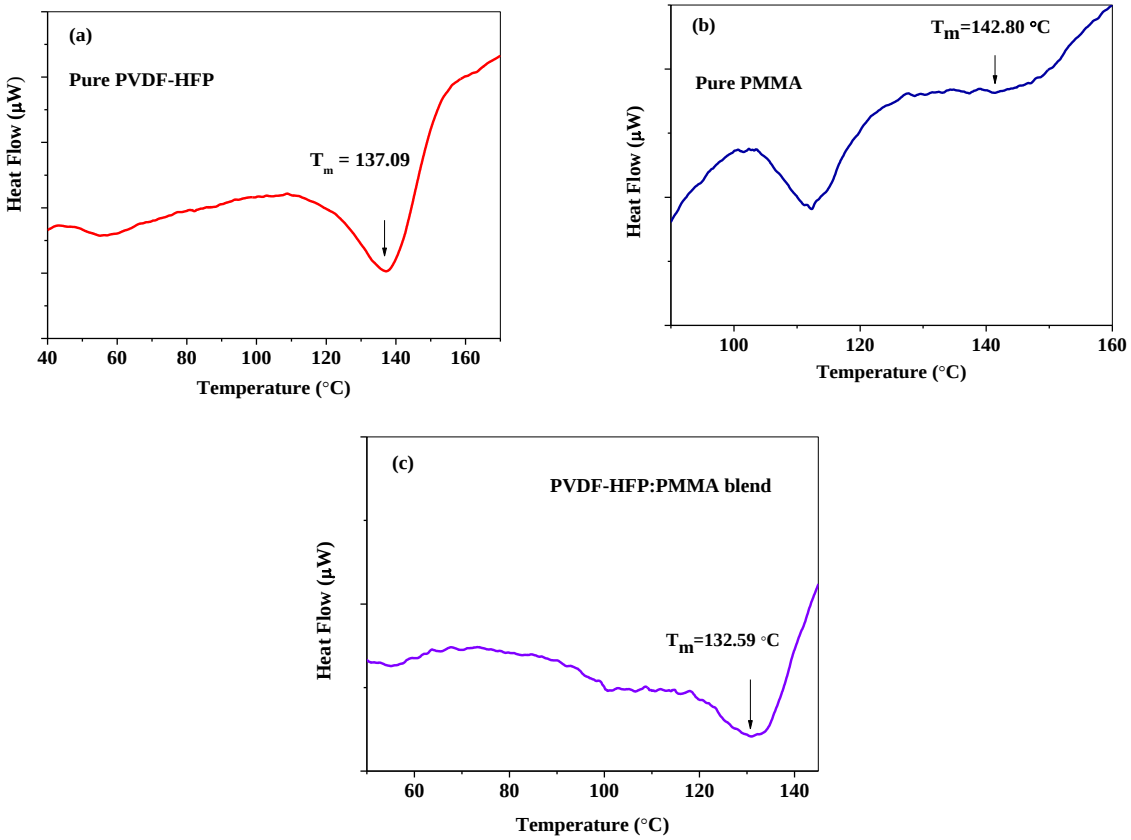

Figure 4.9 DSC thermogram of (a) pure PVDF-HFP (b) pure PMMA (c) PVDF-HFP:PMMA blend

Figure 4.10 represents the DSC profile of PVDF-HFP:PMMA-PC:DEC-$LiClO_4$ gel polymer electrolyte with a varying salt concentration of 2 wt.% to 10 wt.% respectively. As discussed above, the endothermic peak for the PVDF-HFP:PMMA blend is observed at 132.59 °C corresponds to the melting temperature of the blend. With the addition of 2 wt.% $LiClO_4$, the melting peak of GPE has been shifted to 128.86 °C. With further increase of the $LiClO_4$ salt concentration, the peak is observed to shift further towards the lower temperature side. The melting peak of the GPE system with the 7.5 wt.% $LiClO_4$ has been found at 119.62 °C, the lowest temperature. The interaction between Li^+ ion and polymer chains prevents the polymer chain to crystallize and achieve an amorphous-like state. Ibrahim et al. reported the continuous decrease in the crystallinity and melting temperature of the electrolyte system with the addition of $LiPF_6$ from 0 wt.% to 20 wt.%

into PEO polymer matrix [19]. In our case, the peak is shifted towards the higher temperature side instead of the lower side upon addition of 10 wt.% $LiClO_4$ into GPE, and an endothermic peak of melting temperature is observed at 124.57 °C. This shift indicates the stiffness and crystalline nature of the film, increases due to the interaction of $LiClO_4$ with the polymer matrix which is also revealed in X-ray analysis [20]. Ramesh et al. reported the decrease in T_m by the incorporation of LiTf in PVDF-HFP polymer [21]. According to Ramesh et al., the decreased melting temperature is a result of change in the crystalline nature of the sample or localized influence of the polymer chain conformation of the system.

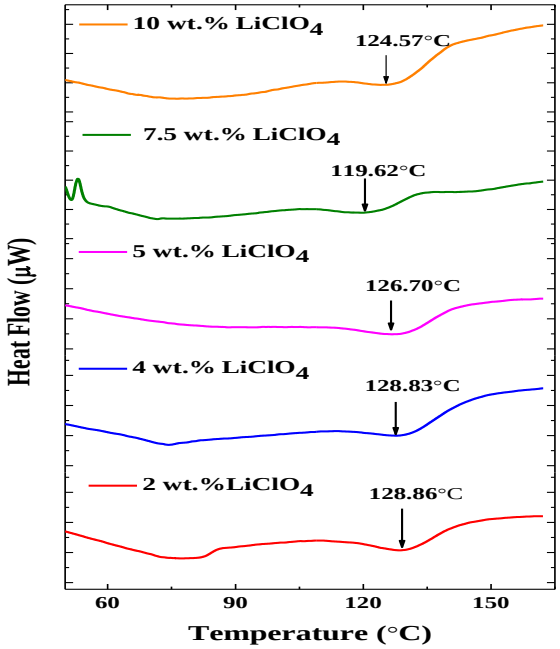

Figure 4.10 DSC thermograph of GPE system with different concentrations of $LiClO_4$ - Series (a).

The DSC result indicates the change in plasticizer variation affects the melting temperatures of the system when PC and DEC plasticizers are taken in a 1:1 ratio in PVDF-HFP:PMMA – $LiClO_4$ – x wt.% PC:DEC (1:1) GPE system. The DSC thermogram has shown a decrease in melting temperature as shown in Figure 4.11. For the system with a low amount of plasticizers i.e. 20 wt.%, the melting point is recorded at 132.33 °C which is slightly below the recorded melting temperature (132.59 °C) of the blend. It is clear from that Figure 4.11, the endothermic peaks continuously shift to lower temperatures side with the increase in the amount of PC: DEC from 20 wt.% to 60 wt.%. This indicates an

enhancement in the flexibility of the polymer chain and increases in the randomness of the chains [22]. Hence lithium-ion motion takes place easily through this flexible and random arrangements of the polymer chains which facilitates increment in ionic conductivity [23]. According to Song et al., the addition of plasticizers causes dipole-dipole interactions between polymer chain segments and both salt and plasticizer, leading to a decrease in the melting point of the electrolyte films [9]. The melting temperature of GPE film with the highest amount of PC:DEC plasticizers still ~ 122.33°C enough for the film to be used as a separator for a battery application.

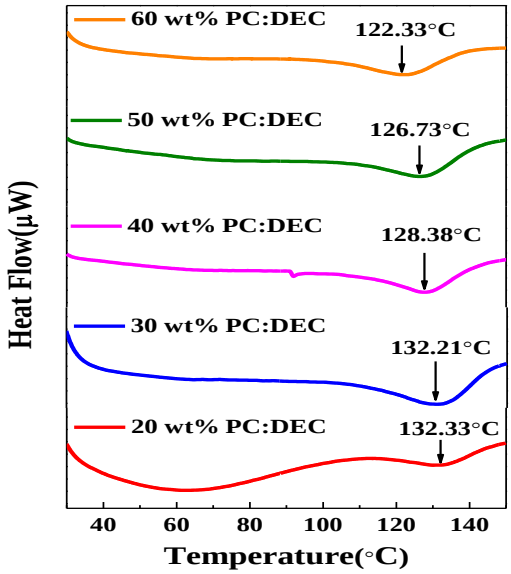

Figure 4.11 DSC thermograph of GPE system with different concentrations of PC:DEC - Series (b).

The effect of Al_2O_3 nano-filler variation in gel polymer electrolyte systems is observed by DSC. The amount of Al_2O_3 nanofiller is varied from 0.5 wt.% to 4 wt.% in the optimized system from the second series i.e. PVDF-HFP:PMMA-10 wt.% $LiClO_4$-60 wt.% PC:DEC. Figure 4.12 shows the DSC thermograph of PVDF-HFP: PMMA-10 wt.% $LiClO_4$-60 wt.% PC: DEC- x wt.% Al_2O_3, where x = 0.5, 1, 2, 3, 4. In an optimized system which is having a melting peak at 122.33°C, the incorporation of 0.5 wt.% Al_2O_3 nanofiller leads to an increase in melting temperature consistent with the enhanced mechanical behavior of the system [24]. With increasing the amount of nano-filler Al_2O_3, the melting peak shifts towards lower temperatures up to 2 wt.% Al_2O_3. The decrease in the melting temperature is a result of the increased amorphous nature of the chain arrangements because the

addition of nano-filler weakens the intermolecular interaction between polymer-polymer and between ion-ion i.e. Li^+ and ClO_4^- ions resulting in enhancement of amourphicity of the system. At 3 wt.% Al_2O_3, the melting point is observed at a higher temperature indicating the increased stiffness of the polymer film. At a higher amount of Al_2O_3, the filler ion aggregation leads to an increase in the crystalline nature.

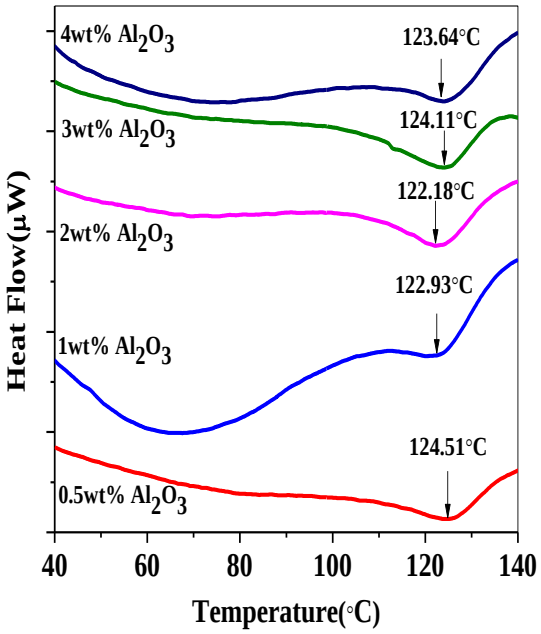

Figure 4.12 DSC thermograph of nanocomposite GPE system with different concentration of Al_2O_3 - Series (c).

4.4 FTIR Analysis

The transport of lithium ions through the polymer matrix depends on the interaction between ion-ion, ion-polymer, and various groups present. FTIR spectra are able to show the complexation and interaction among the various constituents present in gel polymer electrolyte systems. To identify the different types of bonding, functional group, and to examine the changes in them due to interaction among atoms/molecules and ions in the present electrolyte system, FTIR analysis has been done. The interaction occurring among the atoms or ions can cause a change in the vibrational modes of molecules present in the system. Hence, change in bond length or its vibration between polymer-ion, ion-ion, or

due to complexation taking in the polymer electrolyte can be studied by the FTIR technique.

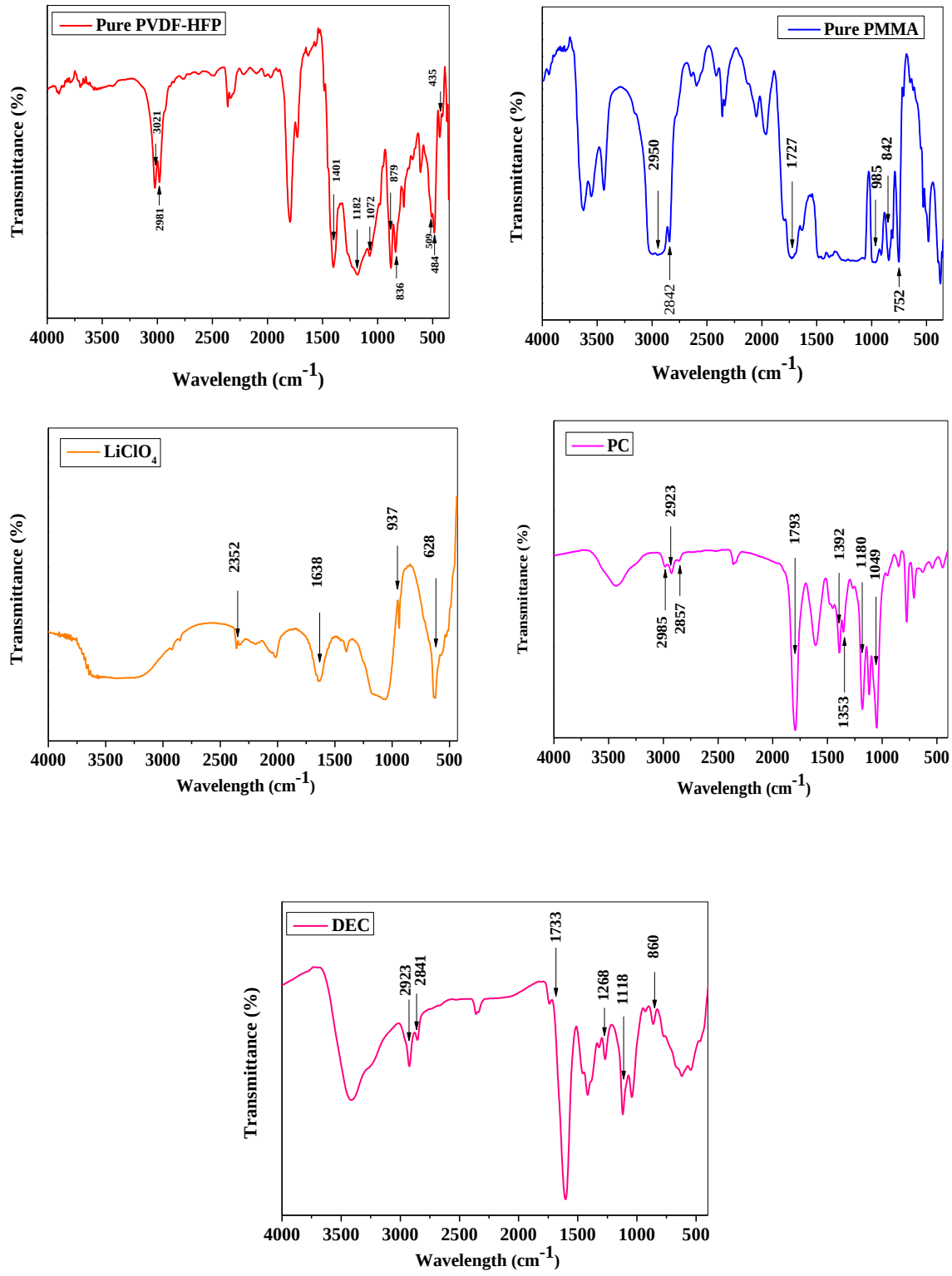

Figure 4.13 FTIR spectra of pure PVDF-HFP, pure PMMA, $LiClO_4$, PC, and DEC

Table 4.1 Characteristic frequencies of pure PVDF-HFP, pure PMMA, $LiClO_4$, PC, and DEC.

Materials	**Wave numbers (cm^{-1})**	**Assignment of Bands**
PVDF-HFP	484,435	CF_2 wagging [25]
	509	CF_2 bending [25]
	879,836	The vibration of the amorphous phase [25]
	1401,1182,1072	α crystalline phase [25]
	2981	Symmetrical stretching of CH_2 group [25]
	3021	Non-symmetrical stretching of CH_2 group [25]
PMMA	752	CH_2 rocking with skeleton stretching [26]
	842	C-H rocking vibration [26]
	985	Symmetric stretching C-O bond [26]
	1727	Symmetric stretching of carbonyl group C=O [26]
	2842, 2950	CH_3 asymmetric stretching [26]
$LiClO_4$	628	stretching vibration of ClO_4^- [27]
	937	Symmetrical vibration of ionic pairs between Li^+ and ClO_4^- [27]
	1638, 2352	Stretching and bending vibration of OH bonds for absorbing water [27]
PC	1049,1180	C–O stretch group [28,29]
	1793	Carbonyl group C=O [28,29]
	1353,1392	C–H bending [28,29]
	2857	$–CH_2$ stretching [28,29]
	2923,2985	$–CH_3$ stretching [28,29]
DEC	860	CH_2 rocking [30]
	1118	CH_3 rocking [30]
	1268	O–C–O asymmetric stretching [30]
	1733	carbonyl group C=O stretching [30]
	2841	CH_3 asymmetric stretching [30]
	2923	CH_2 asymmetric stretching [30]

The FTIR spectra are recorded in the wavenumber range 400-4000 cm^{-1} for all systems. The FTIR spectra of pure PVDF-HFP, pure PMMA, $LiClO_4$, PC, DEC is shown in Figure 4.13. The characteristic frequencies of fundamental vibrational modes correspond to the wavenumber of pure elements collected from the FTIR spectra are listed in Table 4.1.

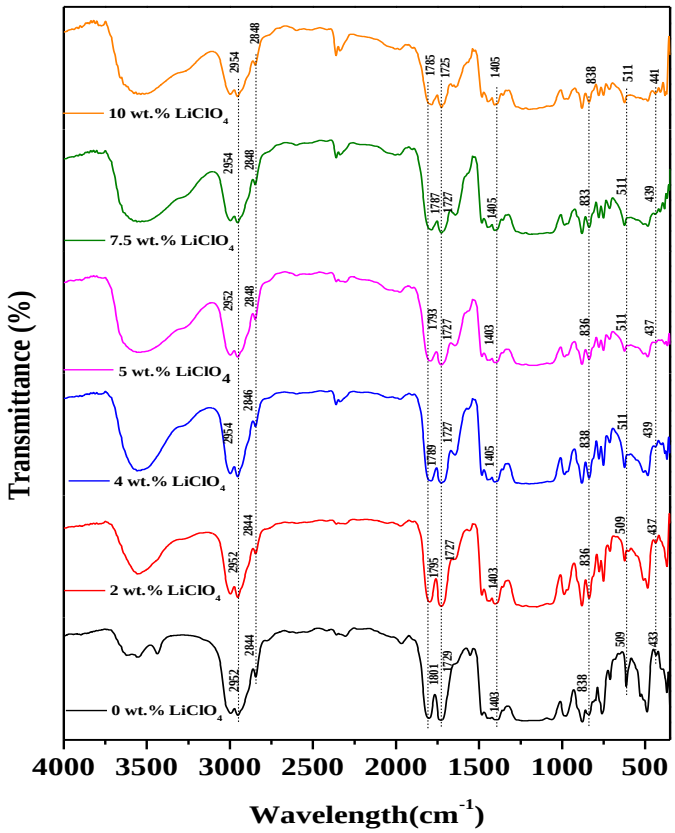

Figure 4.14 FTIR spectra of GPE with different concentrations of $LiClO_4$ - Series (a).

PVDF-HFP holds free electron pairs at the fluorine (F) atoms of CF_2 and CF_3 groups [31]. The absorption frequency appeared at 509 cm^{-1} and 435 cm^{-1} are assigned to the bending and wagging vibrations of $–CF_2$, respectively, and get shifted to 511 cm^{-1} and 441 cm^{-1}, respectively, with the addition of lithium salt. The characteristic peak of PVDF-HFP at 836 cm^{-1} corresponds to the vibration of the amorphous phase (vinylidene group) shifted to a higher frequency at 838 cm^{-1}. The characteristic bands of PVDF-HFP at 1401 cm^{-1} are broadened, reduced in intensity, and shifted to 1405 cm^{-1} indicates the increase in bond length. Other crystalline peaks at 1182 cm^{-1} and 1072 cm^{-1} of pure PVDF-HFP reduced in intensity and eventually disappearing when blended with PMMA leading to the suppression of semi crystallinity of PVDF-HFP. It has also been observed that the characteristic peak of pure PVDF-HFP at 1795 cm^{-1} is shifted to 1785 cm^{-1}. The peak at 2842 cm^{-1} position associated with CH_3 asymmetric stretching vibration of PMMA gets shifted from 2844 cm^{-1} to 2848 cm^{-1} and band appearing at 1727 cm^{-1} is allocated to the symmetrical stretching of the carbonyl group C=O in the PMMA backbone that shifts the band toward the lower side of the frequency at 1725 cm^{-1} and intensity is reduced

significantly with increasing salt concentrations. This indicates the strong interaction of Li ions with the carbonyl group of PMMA. Shukla et al.[4] also reported the strong interaction between Li^+ and C=O in their FTIR studies of lithium salt polymer complexes. Apart from this, the peak at 2950 cm^{-1} ascribed to CH_3 asymmetric stretching is shifted to 2954 cm^{-1} in the complexes. In addition, many of the peaks of the polymer electrolyte system disappeared in the IR spectra. The characteristic peaks of pure $LiClO_4$ are found absent in the polymer electrolyte complexes which confirm good complexation of the salt with host polymers. The disappearance or shifting of frequency from pure polymers shows an interaction of the polymers with salt in GPE samples.

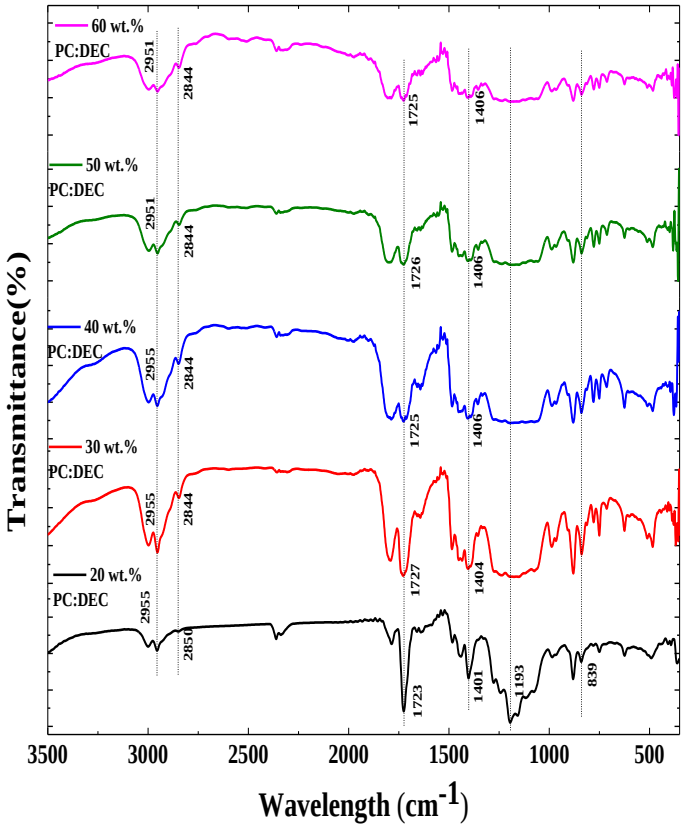

Figure 4.15 FTIR spectra of GPE with different concentrations of PC:DEC - Series (b).

The effect of PC:DEC variation in GPE system has been studied by FTIR which is shown in Figure 4.15. The assigned bending and wagging vibrations of $-CF_2$ of PVDF-HFP at 509 cm^{-1} and 435 cm^{-1} get shifted to higher wavenumbers 511 cm^{-1} and 440 cm^{-1} respectively with an increasing amount of PC:DEC. The vibration at 879 cm^{-1} and 836 cm^{-1} exhibited by PVDF−HFP is observed to shift to a higher frequency at 880 $cm^{-1}$and 838 cm^{-1} respectively. The peak at 1401 cm^{-1} is getting broadened with the reduction in

intensity and shifted to 1403 cm^{-1}, specifying that interaction between polymers and plasticizers as well as salt has taken place and the intensity of other peaks at 1072 cm^{-1} and 1182 cm^{-1} of pure PVDF−HFP get reduced and becomes flatten indicating the increased amorphousity with the addition of more amount of PC:DEC plasticizers. The characteristic peak at 2981 cm^{-1} is ascribed to symmetrical stretching of CH_2 group of pure PVDF−HFP is shifted towards lower frequency side. The CH_3 asymmetric stretching vibration of PMMA at 2842 cm^{-1} shifts to 2846 cm^{-1}. The C = O group (carbonyl group) of PMMA at 1727 cm^{-1} shifts towards the lower frequency side at 1725 cm^{-1} and at the same time intensity is reduced significantly upon the addition of PC:DEC plasticizers. This suggests that the occurrence of the strong interaction between Li^+ and the carbonyl group of PMMA with the addition of plasticizers because when low molecular plasticizers are added to polymer results in dissociation of salt. Apart from these, the intensity of many other peaks has been found to be reduced significantly. This indicates complex formation and increased randomness in polymer chains take place [32].

In the next study, the effect of Al_2O_3 in an optimized GPE system with plasticizers and salt $LiClO_4$ in the blend polymer complex is examined. As can be seen from the Figure 4.16, no significant change has been seen, however, on close inspection, few changes of the broadening of the band of few functional groups have been observed. The band between 1054 cm^{-1} - 1272 cm^{-1} corresponds to C–O stretching and O–C–O asymmetric stretching of PC and DEC becoming broadening with Al_2O_3 because of the strong affinity of PC/DEC towards Al_2O_3 which leads to the formation of stretched Al–O–C bond in the nanocomposite gel polymer electrolyte. The bonds of C=O of PMMA, PC, and DEC near ~1700 cm^{-1} have been found to be shifted to 1785 and 1729 cm^{-1} along with broadening which is an indication of interaction amongst the Al_2O_3, plasticizers, polymer, and $LiClO_4$. At the same time intensity is reduced significantly upon the addition of nano-filler up to 2 wt.% Al_2O_3. The characteristic peak at 2981 cm^{-1} is ascribed to symmetrical stretching of CH_2 group of pure PVDF−HFP is shifted towards higher wavenumber 2994 cm^{-1}. CH_3 asymmetric stretching at 2842 cm^{-1} of PMMA and DEC has been shifted to 2846 cm^{-1}. These observations indicate the elongation of the bond due to the interaction between the ion-filler-polymer is taking place.

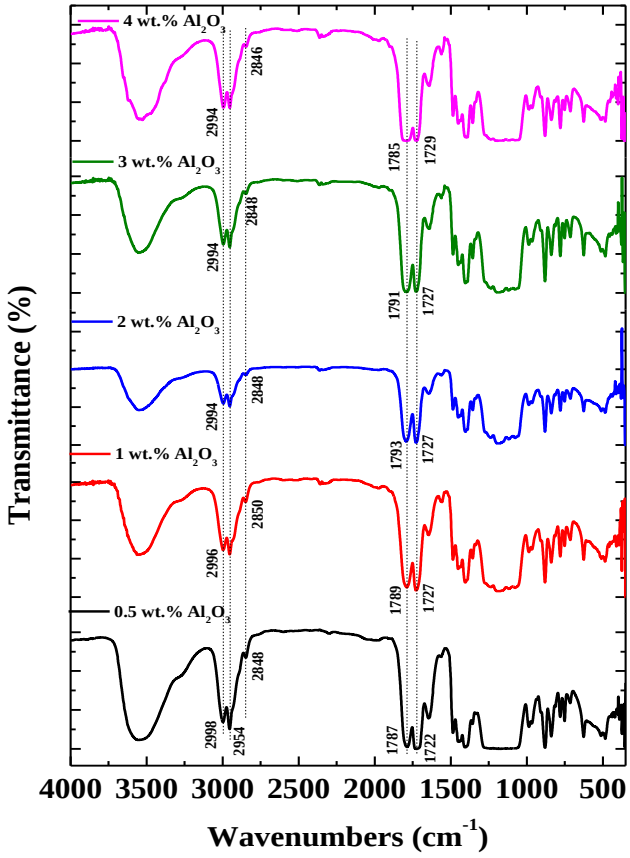

Figure 4.16 FTIR spectra of nanocomposite GPE with different concentrations of Al_2O_3-Series (c).

4.5 AFM Analysis

In the present study, AFM is used to study the morphological properties of prepared GPE films.

Figure **4.17** shows the AFM images of the GPE system (Series a) containing 7.5 wt.% and 10 wt.% $LiClO_4$. On varying $LiClO_4$ salt concentrations within the GPEs, significant morphological changes are seen in terms of roughness events. For GPE system with 7.5 wt.% $LiClO_4$, the maximum roughness height in AFM graphs is observed of 6.3 μm. The maximum roughness height drastically rises to 18.2 μm upon addition of the salt amount of 10 wt.%. This rise may be due to the salt ion aggregation results in the blocking effect [33]. A similar kind of observation was also reported by Maheshwaran et al. in their study of PEO + EMIM-BF_4 for the different concentrations of $Mg(CF_3SO_3)_2$ [34].

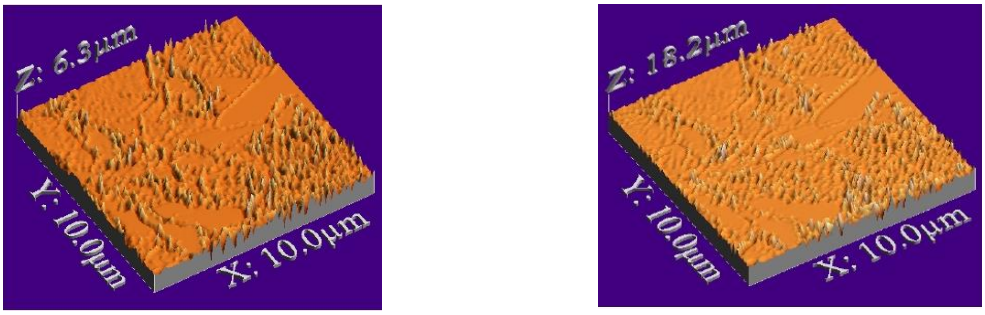

(a) 7.5 wt.% $LiClO_4$ (b) 10 wt.% $LiClO_4$

Figure 4.17 AFM images of GPE having (a) 7.5 wt.% and (b) 10 wt.% $LiClO_4$ - Series (a).

Three-dimensional topographical images of the GPE system (Series b) containing 30 wt.% and 60 wt.% PC:DEC is shown in Figure 4.18. In the three-dimensional view of the topography image, well-defined mountain valleys have been observed. The average roughness height values are found to be decreased from 1.35 µm and 239 nm as the plasticizer amount changes from 30 wt.% and 60 wt.% indicating an increase in the smoothness. This smooth surface is mainly due to entrapped electrolytes within the pores causes modifications in the surface topology which are responsible for easy ionic movement. A similar effect has also been reported by Subbu et al. [32] for PEO/PVdC-co-AN/$LiClO_4$/EC-based systems.

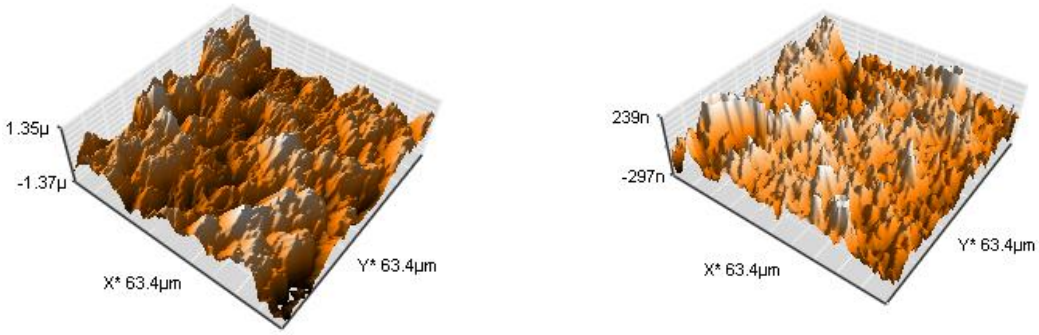

(a) 30 wt.% PC:DEC (b) 60 wt.% PC:DEC

Figure 4.18 AFM images of GPE having (a) 30 wt.% and (b) 60 wt.% PC:DEC - Series (b).

Figure 4.19 depicts the AFM images for electrolyte films with 0.5 wt.% and 2 wt.% Al_2O_3 nano-particles in GPE matrix (Series c). A significant change in the morphology of GPE system has been observed when the content of Al_2O_3 is varied. As the Al_2O_3 concentration is changed from 0.5 wt.% to 2 wt.%, the maximum roughness height decreases from 791.0

nm to 732.7 nm and a relatively smooth surface has been observed. we can also note that the Al_2O_3 nanoparticles are perfectly dispersed in the polymer matrix. The decrease in the roughness height in $MgTf_2$/PEO/PC-DEC/MgO matrix as the MgO nanoparticle is varied from 0 wt.% to 1 wt.% has also been observed by Maheshwaran et al.[35].

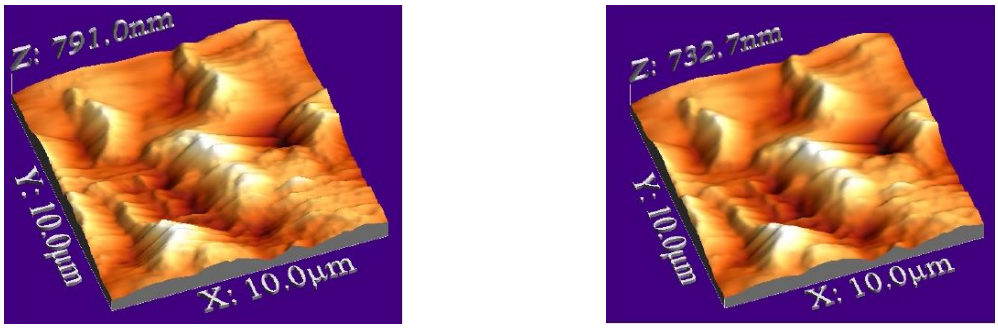

(a) 0.5 wt.% Al_2O_3 (b) 2 wt.% Al_2O_3

Figure 4.19 AFM images of GPE having (a) 0.5 wt.% and (b) 2 wt.% Al_2O_3- Series (c).

4.6 Transport Number Measurement

As discussed in chapter 1, the high ionic conductivity is an essential property of an electrolyte to be used in electrochemical devices. The high ionic conduction mechanism is governed by few ionic transport parameters i.e. ionic conductivity (σ), mobility of ions (μ), carrier concentration (n), drift velocity (v_d), high ionic transference number (t_{ion}). Hence, it is also imperative to have t_{ion} measurement, which is measured by Wagner's polarization method also called Wagner's DC polarization technique. The fraction of the total current carried by an electrolyte due to ionic species is known as transport number also called transference number. The performance of a device highly depends on the properties of the polymer electrolyte and the measure of transference number. The pure ionic conductor follows Ohm's law i.e. the total current is directly proportional to applied DC potential (V_{DC}) across the sample when the applied potential is less than the decomposition potential of the specimen. Hence, DC polarization is an appropriate method to explain the ion transport behavior of ionic conductors or superionic solids. The transference number gives quantitative information regarding ionic and electronic contribution to the total ionic conductivity, it is given as,

$$t_i = \frac{i_t - i_e}{i_t} = 1 - \frac{i_e}{i_t} = 1 - t_e \qquad (4.1)$$

where t_i = ionic transport number, σ_i and σ_t are conductivity due to ions and total conductivity (ionic + electronic), respectively. i_i and i_t are current due to ions and total current (ionic + electronic).

Wagner's DC polarization technique was used by Watanabe et al.[36] in Transient Ionic Current(TIC) technique, in which both electrodes were blocking instead of one blocking and other non-blocking. In this technique, initially, the sample is polarized by applying a constant DC voltage for sufficient time. After the achievement of complete polarization, the polarity of the applied voltage is reversed. In this situation, the polarization ion clouds travel to opposite electrolytes through the bulk electrolyte and current flow. The current was being measured simultaneously with time. From the recorded values, the ionic transport number is calculated using Eq. 4.1 . Especially, when the polymer electrolytes are used for battery application, the main charge carriers should be ion. This means, the ionic transport number should be close to unity (close to one) and electronic contribution towards conductivity should be negligible (close to zero).

Table 4.2 Ionic transport number for different GPE systems

Samples	t_i	t_e
Series (a) : PVDF-HFP:PMMA-$LiClO_4$-PC:DEC with different concentrations of $LiClO_4$		
2 wt.% $LiClO_4$	0.97	0.03
4 wt.% $LiClO_4$	0.96	0.04
5 wt.% $LiClO_4$	0.99	0.01
7.5 wt.% $LiClO_4$	0.99	0.01
10 wt.% $LiClO_4$	0.97	0.03
Series (b): PVDF-HFP:PMMA-$LiClO_4$-PC:DEC with different concentrations of PC:DEC		
20 wt.% PC:DEC	0.97	0.03
30 wt.% PC:DEC	0.97	0.03
40 wt.% PC:DEC	0.99	0.01
50 wt.% PC:DEC	0.98	0.02
60 wt.% PC:DEC	0.99	0.01
Series (c): PVDF-HFP:PMMA-$LiClO_4$-PC:DEC-Al_2O_3 with different concentrations of Al_2O_3		
0.5 wt.% Al_2O_3	0.99	0.01
1 wt.% Al_2O_3	0.98	0.02
2 wt.% Al_2O_3	0.99	0.01
3 wt.% Al_2O_3	0.99	0.01
4 wt.% Al_2O_3	0.99	0.01

In the present study, the transport number is measured for all series of gel polymer electrolytes using Wagner's DC polarization technique [37]. In this technique, the

polarization current was monitored as a function of time upon the application of a fixed DC voltage across the SS/GPE/SS cell. The typical curve for measured current versus time data is plotted and discussed in Chapter 3. The ionic transport numbers are calculated from the polarization current versus time plot by using Eq. 4.1 and the calculated transport numbers are listed in Table 4.2. For all the polymer gel electrolyte systems, the values of the ionic transport number are measured in the range of 0.96–0.99, and electronic contribution is found to be very less that is 0.01 to 0.03. From the observed value, one can say, the present gel polymer electrolyte is a highly ionic conductor. This suggests that the charge transport in these polymer electrolytes is mainly due to ions and only a negligible contribution comes from electrons [38].

4.7 Electrochemical Stability Window

From the point of view of the application of polymer electrolyte in the battery, high conductivity is an essential property, but it is also necessary to measure the electrochemical stability window of an electrolyte [32]. The electrochemical stability window (ESW) is defined as the working voltage (potential) range of a substance [31]. The difference between oxidation and reduction potential gives the stability window of material from the cyclic voltammetry (CV) profile. The electrochemical stability window of the GPE system was measured by linear sweep voltammetry (LSV). The test of GPE film exhibiting maximum ionic conductivity was done at a scan rate of 50 mV/s and the measurement configuration for the same is SSE/GPE/SSE, where SSE is a stainless-steel electrode. The measured electrochemical stability window values for different gel polymer electrolyte systems are tabulated in Table 4.3.

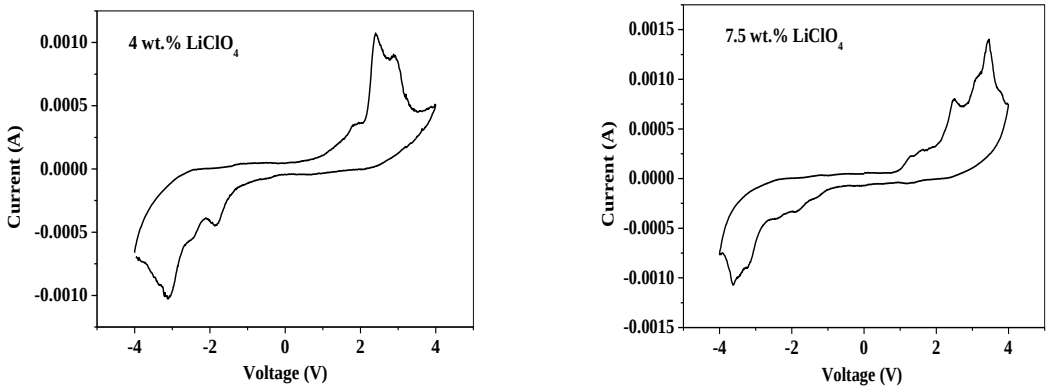

Figure 4.20 Cyclic voltammogram of GPE having 4 wt.% and 7.5 wt.% $LiClO_4$ - Series (a).

The Cyclic Voltammogram of GPE having 4 wt.% and 7.5 wt.% $LiClO_4$ is shown in Figure 4.20. The electrochemical stability window for the GPE system (series (a)) with 4 wt.% and 7.5 wt.% of $LiClO_4$ has been recorded. The recorded stability windows are ≈ 4.31 V and ≈ 4.40 V respectively. It can also be seen from the figure that the stability of the GPE sample with 7.5 wt.% $LiClO_4$ is high.

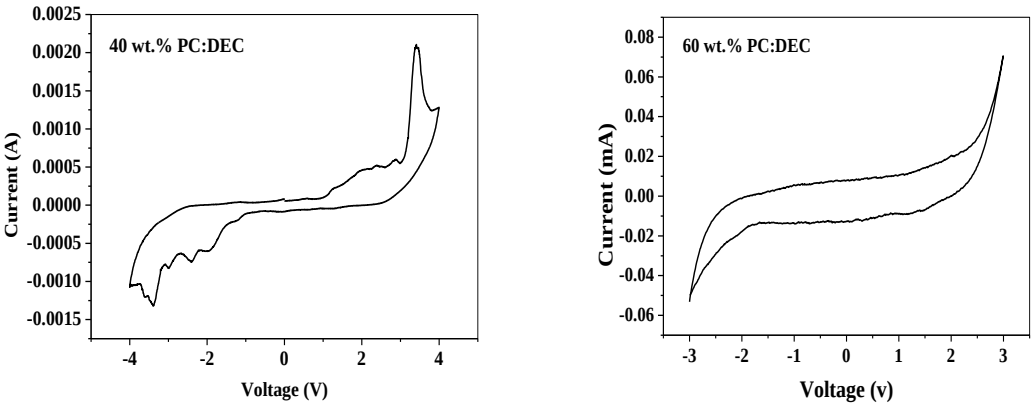

Figure 4.21 Cyclic Voltammogram of GPE having 40 wt.% and 60 wt.% PC:DEC - Series (b).

Next, the plasticizer variation GPE system (series (b)), the gel polymer electrolyte sample with 40 wt.% and 60 wt.% PC:DEC were undergone for the linear sweep voltammetry study. The cyclic voltammogram is depicted in Figure 4.21. The electrochemical stability was found of ≈ 4.20 V and ≈ 4.89 V respectively. The highest conducting sample having 60 wt.% PC: DEC has a high stability window of ≈ 4.89 V which is greater than the observed window of ≈ 4.40 V of high conducting sample of series (a). Bose et al. have reported an electrochemical stability window of 4.2 V for the gel polymer electrolyte comprised of PVDF-HFP-LITFSI-EC:DMC [39]. The electrochemical stability window of ≈ 4.5 V for the PVDF-HFP-EC:DEC-$LiClO_4$ system has been reported by Liu et al. [39].

It is believed that the addition of nano-filler in the polymer electrolytes improves the electrochemical properties especially high stability window, compatibility with lithium electrode, etc. [40]. Next from the third series, the LSV test was done for the nanocomposite gel polymer electrolyte containing 1 wt.% Al_2O_3 and 2 wt.% Al_2O_3 (Figure 4.22). The recorded stability windows are ≈ 5.67 V and ≈ 6.00 V, respectively. Among all samples, the NCGPE with 2 wt.% Al_2O_3 is found to have the highest electrochemical

stability window. This indicates on the addition of Al_2O_3 nano-filler, the stability window increases up to ≈ 6.00 V, which is a sufficient voltage range for the electrochemical application, particularly meeting the actual need of lithium batteries. Zhao et al. reported the addition of GO (graphene oxide) as a filler in GPE to broaden the electrochemical stability window of ≈ 4.85 V electrolyte membrane [41].

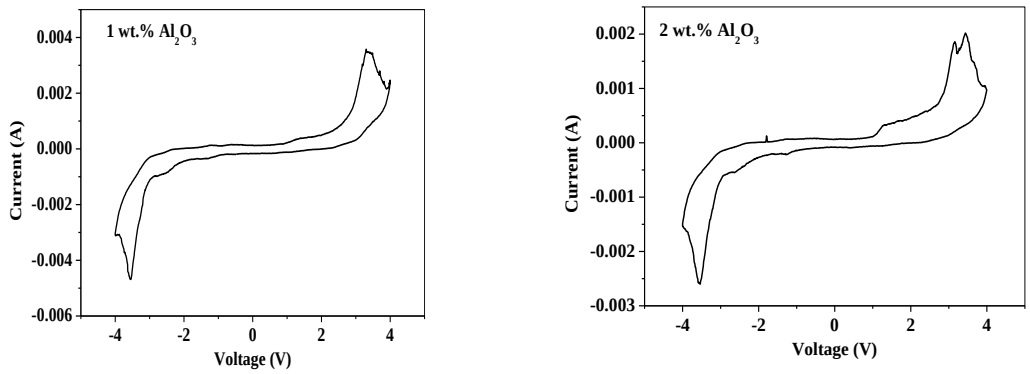

Figure 4.22 Cyclic voltammogram of nanocomposite GPE having 1 wt.% and 2 wt.% Al_2O_3 – Series (c).

Table 4.3 Electrochemical stability window of different gel polymer electrolyte systems.

Series	Samples	Electrochemical stability window (V)
Series (a)	4 wt.% $LiClO_4$	4.31
Series (a)	7.5 wt.% $LiClO_4$	4.40
Series (b)	40 wt.% PC:DEC	4.20
Series (b)	60 wt.% PC:DEC	4.89
Series (c)	1 wt.% Al_2O_3	5.67
Series (c)	2 wt.% Al_2O_3	6.00

4.8 Mechanical Strength

The gel polymer electrolyte plays an important role as a separator between the electrodes under pressure in the battery application. The mechanical properties of the gel polymer electrolyte are an important factor in terms of the long-life cycle. The gel polymer electrolyte has high ionic conductivity but also possesses a large amount of liquid electrolytes which deteriorates its mechanical integrity. Furthermore, the gel polymer electrolyte membrane for the electrochemical applications must have a balance between its ionic conductivity and mechanical strength i.e. excellent ionic conductivity and

mechanical strength. The tensile tests are done to investigate the mechanical properties of the GPE films of all series.

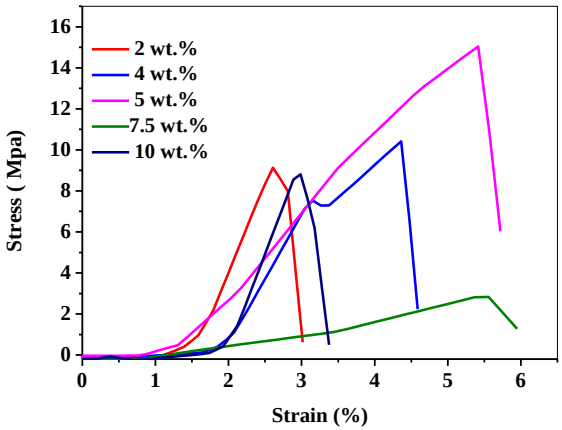

Figure 4.23 Stress-strain curve of GPE with different concentrations of $LiClO_4$ –Series (a).

The stress-strain curve for the gel polymer electrolyte with different concentrations of $LiClO_4$ salt is shown in Figure 4.23. The mechanical strength is varying with the change in the concentration of $LiClO_4$ in gel polymer electrolyte systems. The sample with 7.5 wt.% $LiClO_4$ having good electrical properties has critical stress of 2.76 MPa with an elongation at a break value of 5.56%. The value of breaking strength ≈ 2.76 MPa is very low which is not suitable for the battery application.

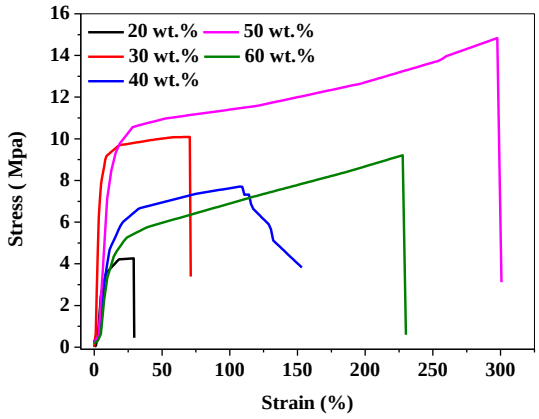

Figure 4.24 Stress-strain curve of GPE with different concentrations of PC:DEC – Series (b).

Next, the effect of PC:DEC plasticizers variation on mechanical strength has been studied. The stress-strain curve for the gel polymer electrolyte system with different concentrations of PC: DEC is shown in Figure 4.24. The mechanical strength is very low for the GPE sample with 20 wt.% PC:DEC. For this sample, the breaking stress ~ 4.28 MPa with an elongation at break ≈ 28 %. At higher concentration of plasticizers i.e. 50 wt.% PC:DEC, the critical stress 14.86 MPa and elongation at break 297% with good elasticity which is

much larger among all the samples of this series b. But, when 60 wt.% plasticizers are added to the film, both critical stress and elongation at break significantly get lower. The breaking stress ≈ 9.21 MPa and elongation at break ≈ 227 % have been observed. However, the GPE membrane with 60 wt.% PC:DEC shows good electrical properties. It can be concluded that the good electrical properties possessed by the sample with 60 wt.% PC:DEC at the cost of degradation in the mechanical strength of the membrane. The decrease in the critical stress and elongation at break at higher the amount of plasticizers in PVDF-HFP based polymer electrolyte systems has also been reported by Fan et al. [42].

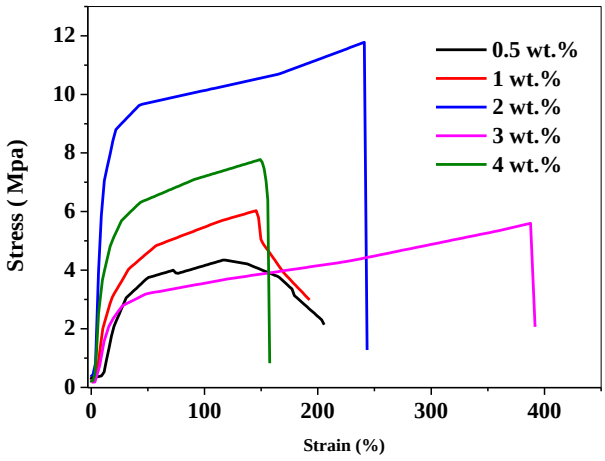

Figure 4.25 Stress-strain curve of nanocomposite GPE with different concentrations of Al_2O_3 –Series (c).

To avoid the compromise between mechanical properties and ionic conductivity in the gel polymer electrolyte, the strategies of incorporation of nano-filler in the GPE have been adopted [43,44]. Next, the effect of Al_2O_3 nano-filler variation on the mechanical strength of the NCGPE has been studied. The stress-strain curve for the nano-composite gel polymer electrolyte at different concentrations of Al_2O_3 nano-fillers is shown in Figure 4.25. Upon addition of nano-filler to GPE, the mechanical strength is found to be varied. As the concentration of Al_2O_3 is varied from 0.5 to 2 wt.%, the mechanical strength is found to be improved. For nano-composite gel polymer electrolyte with 2 wt.% Al_2O_3 with good electrical property, the breaking stress value of ≈ 11.78 MPa, and impressive extensibility with elongation at break ≈ 243 % have been recorded. Both values are larger than the sample with 60 wt.% PC:DEC from series (b). The enhancement in the mechanical properties of this sample could be attributed to the interaction between the Al_2O_3 nano-filler with the polymer matrix. The enhancement in mechanical strength by

incorporating MMT nanoclay in PVDF-HFP/PMMA based polymer electrolytes has also been found by Zhang et al. in their study [45]. On further addition Al_2O_3, either breaking stress or elongation at break is decreasing.

References

[1] R. Muchakayala, S. Song, S. Gao, X. Wang, and Y. Fan, "Structure and ion transport in an ethylene carbonate-modified biodegradable gel polymer electrolyte," *Polym. Test.*, vol. 58, pp. 116–125, 2017, doi: https://doi.org/10.1016/j.polymertesting.2016.12.014.

[2] A. M. Stephan, K. S. Nahm, M. Anbu Kulandainathan, G. Ravi, and J. Wilson, "Poly(vinylidene fluoride-hexafluoropropylene) (PVdF-HFP) based composite electrolytes for lithium batteries," *Eur. Polym. J.*, vol. 42, no. 8, pp. 1728–1734, 2006, doi: https://doi.org/10.1016/j.eurpolymj.2006.02.006.

[3] A. Ayya Nadar, K. Pandian, J. Saravanan, J. S, and B. Sundaresan, "Investigation of the Structural, Electrical and Morphological properties of Mg^{2+} ion conducting Nanocomposite Solid Polymer Electrolytes based on PMMA," *Int. J. Innov. Res. Sci. Eng. Technol.*, vol. 2, p. 4883, Sep. 2013.

[4] N. Shukla and A. K. Thakur, "Role of salt concentration on conductivity optimization and structural phase separation in a solid polymer electrolyte based on PMMA-$LiClO_4$," *Ionics (Kiel).*, vol. 15, no. 3, pp. 357–367, 2009, doi: 10.1007/s11581-008-0275-3.

[5] M. Ulaganathan, R. Nithya, S. Rajendran, and S. Raghu, "Li-ion conduction on nanofiller incorporated PVdF-co-HFP based composite polymer blend electrolytes for flexible battery applications," *Solid State Ionics*, vol. 218, pp. 7–12, 2012, doi: https://doi.org/10.1016/j.ssi.2012.04.029.

[6] O. Mahendran and S. Rajendran, "Ionic conductivity studies in PMMA/PVdF polymer blend electrolyte with lithium salts," *Ionics (Kiel).*, vol. 9, no. 3, pp. 282–288, 2003, doi: 10.1007/BF02375980.

[7] P. Pradeepa, S. Edwin raj, G. Sowmya, J. Kalaiselvimary, and M. Ramesh Prabhu, "Optimization of hybrid polymer electrolytes with the effect of lithium salt concentration in PEO/PVdF-HFP blends," *Mater. Sci. Eng. B*, vol. 205, pp. 6–17, 2016, doi: https://doi.org/10.1016/j.mseb.2015.11.009.

[8] P. Pal and A. Ghosh, "Dynamics and relaxation of charge carriers in poly(methylmethacrylate)-lithium salt based polymer electrolytes plasticized with ethylene carbonate," *J. Appl. Phys.*, vol. 120, no. 4, p. 45108, Jul. 2016, doi: 10.1063/1.4959985.

[9] S. Song, J. Wang, J. Tang, R. Muchakayala, and R. Ma, "Preparation, properties, and Li-ion battery application of EC + PC-modified PVdF-HFP gel polymer electrolyte films," *Ionics (Kiel).*, vol. 23, no. 12, pp. 3365–3375, 2017, doi: 10.1007/s11581-017-2130-x.

[10] S. Choudhary and R. J. Sengwa, "Effects of different inorganic nanoparticles on the structural, dielectric and ion transportation properties of polymers blend based nanocomposite solid polymer electrolytes," *Electrochim. Acta*, vol. 247, pp. 924–941, 2017, doi: https://doi.org/10.1016/j.electacta.2017.07.051.

[11] M. Moskwiak *et al.*, "Physico- and electrochemistry of composite electrolytes based on PEODME–LiTFSI with TiO_2," *J. Power Sources*, vol. 159, no. 1, pp. 443–448, 2006, doi: https://doi.org/10.1016/j.jpowsour.2006.02.040.

[12] K. Mishra, T. Arif, R. Kumar, and D. Kumar, "Effect of Al_2O_3 nanoparticles on ionic conductivity of PVdF-HFP/PMMA blend-based Na+-ion conducting nanocomposite gel polymer electrolyte," *J. Solid State Electrochem.*, vol. 23, no. 8, pp. 2401–2409, 2019, doi: 10.1007/s10008-019-04348-9.

[13] S. Ramesh and S.-C. Lu, "A simple P(VdF-HFP)–LiTf system yielding highly ionic conducting and thermally stable solid polymer electrolytes," *J. Mol. Liq.*, vol. 177, pp. 73–77, 2013, doi: https://doi.org/10.1016/j.molliq.2012.09.018.

[14] M. V Bhute and S. B. Kondawar, "Electrospun poly(vinylidene fluoride)/cellulose acetate/$AgTiO_2$ nanofibers polymer electrolyte membrane for lithium ion battery," *Solid State Ionics*, vol. 333, pp. 38–44, 2019, doi: https://doi.org/10.1016/j.ssi.2019.01.019.

[15] P. Senthil Kumar, A. Sakunthala, M. V Reddy, and M. Prabu, "Structural, morphological, electrical and electrochemical study on plasticized PVdF-HFP/PEMA blended polymer electrolyte for lithium polymer battery application," *Solid State Ionics*, vol. 319, pp. 256–265, 2018, doi: https://doi.org/10.1016/j.ssi.2018.02.022.

[16] M. Rao, X. Li, Y. Liao, X. Li, and W. Li, "Preparation and performance of a composite polyimide/poly(vinylidene fluoride-co-hexafluoropropylene)/nano-Al_2O_3 polymer electrolyte for lithium-sulfur cell," *Ionics (Kiel).*, vol. 21, no. 7, pp. 1937–1943, 2015, doi: 10.1007/s11581-014-1360-4.

[17] S. Abbrent, J. Plestil, D. Hlavata, J. Lindgren, J. Tegenfeldt, and Å. Wendsjö, "Crystallinity and morphology of PVdF-HFP-based gel electrolytes," *Polymer (Guildf).*, vol. 42, pp. 1407–1416, Feb. 2001, doi: 10.1016/S0032-3861(00)00517-6.

[18] M. A. Gebreyesus, Y. Purushotham, and J. S. Kumar, "Preparation and characterization of lithium ion conducting polymer electrolytes based on a blend of poly(vinylidene fluoride-co-hexafluoropropylene) and poly(methyl methacrylate)," *Heliyon*, vol. 2, no. 7, p. e00134, 2016, doi: https://doi.org/10.1016/j.heliyon.2016.e00134.

[19] S. Ibrahim, M. M. Yassin, R. Ahmad, and M. R. Johan, "Effects of various $LiPF_6$ salt concentrations on PEO-based solid polymer electrolytes," *Ionics (Kiel).*, vol. 17, no. 5, pp. 399–405, 2011, doi: 10.1007/s11581-011-0524-8.

[20] C. Maheshwaran, K. Mishra, D. K. Kanchan, and D. Kumar, "Mg^{2+} conducting polymer gel electrolytes: physical and electrochemical investigations," *Ionics (Kiel).*, vol. 26, no. 6, pp. 2969–2980, 2020, doi: 10.1007/s11581-020-03459-y.

[21] R. T subramaniam and S.-C. Lu, "Effect of lithium salt concentration on crystallinity of poly(vinylidene fluoride-co-hexafluoropropylene)-based solid polymer electrolytes," *J. Mol. Struct.*, vol. 994, pp. 403–409, May 2011, doi: 10.1016/j.molstruc.2011.03.065.

[22] O. Padmaraj, M. Venkateswarlu, and N. Satyanarayana, "Effect of ZnO filler concentration on the conductivity, structure and morphology of PVdF-HFP nanocomposite solid polymer electrolyte for lithium battery application," *Ionics (Kiel).*, vol. 19, no. 12, pp. 1835–1842, 2013, doi: 10.1007/s11581-013-0922-1.

[23] M. R. Johan, O. H. Shy, S. Ibrahim, S. M. Mohd Yassin, and T. Y. Hui, "Effects of Al_2O_3 nanofiller and EC plasticizer on the ionic conductivity enhancement of solid PEO–LiCF3SO3 solid polymer electrolyte," *Solid State Ionics*, vol. 196, no. 1, pp. 41–47, 2011, doi: https://doi.org/10.1016/j.ssi.2011.06.001.

[24] X. Wang *et al.*, "Preparation and characterization of gel polymer electrolytes using poly(ionic liquids) and high lithium salt concentration ionic liquids," *J. Mater. Chem. A*, vol. 5, no. 45, pp. 23844–23852, 2017, doi: 10.1039/C7TA08233A.

[25] K. B. M. Isa *et al.*, "Lithium ion conduction and ion–polymer interaction in PVdF-HFP based gel polymer electrolytes," *Solid State Ionics*, vol. 268, pp. 288–293, 2014, doi: https://doi.org/10.1016/j.ssi.2014.10.012.

[26] P. Sharma, D. K. Kanchan, and N. Gondaliya, "Effect of ethylene carbonate concentration on structural and electrical properties of PEO–PMMA polymer blends," *Ionics (Kiel).*, vol. 19, no. 5, pp. 777–785, 2013, doi: 10.1007/s11581-012-0797-6.

[27] Z. Li, G. Su, D. Gao, X. Wang, and X. Li, "Effect of Al_2O_3 nanoparticles on the electrochemical characteristics of P(VDF-HFP)-based polymer electrolyte," *Electrochim. Acta*, vol. 49, no. 26, pp. 4633–4639, Oct. 2004, doi: 10.1016/J.ELECTACTA.2004.05.018.

[28] D. Battisti, G. A. Nazri, B. Klassen, and R. Aroca, "Vibrational studies of lithium perchlorate in propylene carbonate solutions," *J. Phys. Chem.*, vol. 97, no. 22, pp. 5826–5830, Jun. 1993, doi: 10.1021/j100124a007.

[29] G. J. Janz, J. Ambrose, J. W. Coutts, and J. R. Downey, "Raman spectrum of propylene carbonate," *Spectrochim. Acta Part A Mol. Spectrosc.*, vol. 35, no. 2, pp. 175–179, 1979, doi: https://doi.org/10.1016/0584-8539(79)80181-6.

[30] J. Wang, Y. Wu, X. Xuan, and H. Wang, "Ion–molecule interactions in solutions of lithium perchlorate in propylene carbonate+diethyl carbonate mixtures: an IR and molecular orbital study," *Spectrochim. Acta Part A Mol. Biomol. Spectrosc.*, vol. 58, no. 10, pp. 2097–2104, 2002, doi: https://doi.org/10.1016/S1386-1425(01)00686-2.

[31] P. Prabakaran and R. P. Manimuthu, "Enhancement of the electrochemical properties with the effect of alkali metal systems on PEO/PVdF-HFP complex polymer electrolytes," *Ionics (Kiel).*, vol. 22, no. 6, pp. 827–839, 2016, doi: 10.1007/s11581-015-1618-5.

[32] C. Subbu, S. Rajendran, K. Kesavan, and R. Premila, "The physical and electrochemical properties of poly(vinylidene chloride-co-acrylonitrile)-based polymer electrolytes prepared with different plasticizers," *Ionics (Kiel).*, vol. 22, no. 2, pp. 229–240, 2016, doi: 10.1007/s11581-015-1535-7.

[33] V. Parthiban, S. Akula, S. G. Peera, N. Islam, and A. K. Sahu, "Proton Conducting Nafion-Sulfonated Graphene Hybrid Membranes for Direct Methanol Fuel Cells with Reduced Methanol Crossover," *Energy & Fuels*, vol. 30, no. 1, pp. 725–734, Jan. 2016, doi: 10.1021/acs.energyfuels.5b02194.

[34] C. Maheshwaran, D. K. Kanchan, K. Gohel, K. Mishra, and D. Kumar, "Effect of $Mg(CF_3SO_3)_2$ concentration on structural and electrochemical properties of ionic liquid incorporated polymer electrolyte membranes," *J. Solid State Electrochem.*, Jan. 2020, doi: 10.1007/s10008-020-04507-3.

[35] C. Maheshwaran, D. K. Kanchan, K. Mishra, D. Kumar, and K. Gohel, "Effect of active MgO nano-particles dispersion in small amount within magnesium-ion conducting polymer electrolyte matrix," *Nano-Structures & Nano-Objects*, vol. 24, p. 100587, 2020, doi: https://doi.org/10.1016/j.nanoso.2020.100587.

[36] M. Watanabe, K. Sanui, N. Ogata, T. Kobayashi, and Z. Ohtaki, "Ionic conductivity and mobility in network polymers from poly(propylene oxide) containing lithium perchlorate," *J. Appl. Phys.*, vol. 57, no. 1, pp. 123–128, Jan. 1985, doi: 10.1063/1.335386.

[37] D. Kumar and S. A. Hashmi, "Ion transport and ion–filler-polymer interaction in poly(methyl methacrylate)-based, sodium ion conducting, gel polymer electrolytes dispersed with silica nanoparticles," *J. Power Sources*, vol. 195, no. 15, pp. 5101–5108, 2010, doi: https://doi.org/10.1016/j.jpowsour.2010.02.026.

[38] D. Kumar and S. A. Hashmi, "Ionic liquid based sodium ion conducting gel polymer electrolytes," *Solid State Ionics*, vol. 181, no. 8, pp. 416–423, 2010, doi:

https://doi.org/10.1016/j.ssi.2010.01.025.

[39] P. Bose, D. Deb, and S. Bhattacharya, "Lithium-polymer battery with ionic liquid tethered nanoparticles incorporated P(VDF-HFP) nanocomposite gel polymer electrolyte," *Electrochim. Acta*, vol. 319, pp. 753–765, 2019, doi: https://doi.org/10.1016/j.electacta.2019.07.013.

[40] Y.-J. Wang and D. Kim, "Crystallinity, morphology, mechanical properties and conductivity study of in situ formed PVdF/$LiClO_4$/TiO_2 nanocomposite polymer electrolytes," *Electrochim. Acta*, vol. 52, no. 9, pp. 3181–3189, 2007, doi: https://doi.org/10.1016/j.electacta.2006.09.070.

[41] X. Zhao, C. Tao, Y. Li, X. Chen, J. Wang, and H. Gong, "Preparation of gel polymer electrolyte with high lithium ion transference number using GO as filler and application in lithium battery," *Ionics (Kiel).*, 2020, doi: 10.1007/s11581-020-03628-z.

[42] L. Fan, Z. Dang, C.-W. Nan, and M. Li, "Thermal, electrical and mechanical properties of plasticized polymer electrolytes based on PEO/P(VDF-HFP) blends," *Electrochim. Acta*, vol. 48, no. 2, pp. 205–209, 2002, doi: https://doi.org/10.1016/S0013-4686(02)00603-5.

[43] Z. Song *et al.*, "Origami lithium-ion batteries," *Nat. Commun.*, vol. 5, no. 1, p. 3140, 2014, doi: 10.1038/ncomms4140.

[44] W. Liu *et al.*, "Stretchable Lithium-Ion Batteries Enabled by Device-Scaled Wavy Structure and Elastic-Sticky Separator," *Adv. Energy Mater.*, vol. 7, no. 21, p. 1701076, Nov. 2017, doi: 10.1002/aenm.201701076.

[45] J. Zhang *et al.*, "Taichi-inspired rigid-flexible coupling cellulose-supported solid polymer electrolyte for high-performance lithium batteries," *Sci. Rep.*, vol. 4, no. 1, p. 6272, 2014, doi: 10.1038/srep06272.